

# Plasmon-Assisted Suppression of Surface Trap States and Enhanced Band-Edge Emission in a Bare CdTe Quantum Dot

Assegid M. Flatae,<sup>\*,[a]</sup> Francesco Tantussi,<sup>[b]</sup> Gabriele C. Messina,<sup>[b]</sup> Francesco De Angelis<sup>[b]</sup>, and Mario Agio<sup>[a,c]</sup>

[a] Laboratory of Nano-Optics and Cμ  
University of Siegen  
57072 Siegen, Germany  
flatae@physik.uni-siegen.de

[b] Istituto Italiano di Tecnologia  
16163 Genova, Italy

[c] National Institute of Optics (INO-CNR)  
50125 Florence, Italy

**Abstract:** Colloidal quantum dots have emerged as a versatile photoluminescent and optoelectronic material. Issues like fluorescence intermittency, non-radiative Auger recombination and surface traps are commonly addressed by growing a wide-bandgap shell around the quantum dot. However, the shell isolates the excitonic wave function and reduces its interaction with nanoscale optical fields, which are instrumental for applications such as charge transport in photovoltaics and lasers. Furthermore, the shell causes a longer emission lifetime, which limits their use for high-speed nanoscale optoelectronics and as photoluminescence probes. Here, we demonstrate a high degree of control on the photophysics of a bare core CdTe quantum dot solely by plasmon-coupling, showing that more than 99% of the surface defect-state emission from a trap-rich quantum dot can be quenched. Moreover, the band-edge state excitonic and biexcitonic radiative recombination rates are enhanced by 676 and 293-fold, respectively. The larger photon emission rate improves the quantum efficiency of the excitonic transition by more than a factor of 3, while the increase of the radiative decay rate of the biexciton prevents Auger non-radiative decay channels, leading to a 10-fold enhancement in the quantum efficiency. Plasmonic coupling represents an effective approach for controlling the quantum dot optical properties, with implications for developing nanoscale thresholdless lasers, light emitting devices and single-photon sources.

Colloidal semiconductor quantum dots (QDs) are promising nanomaterials for modern optoelectronics. The size-tunable electronic structure, cheap solution processing, high photostability at room temperature and high fluorescence quantum yield has led to their integration into devices like light emitting diodes, lasers, solar cells, photodetectors, field-effect transistors and memory elements [1]. Such devices rely on the efficiency of charge transport (e.g., photovoltaics) and the efficiency of radiative recombination of carriers (e.g., lasers and light emitting diodes). However, colloidal QDs exhibit fluorescence intermittency (on/off blinking), Auger recombination and surface traps. Carrier trapping hinders both charge transport and radiative recombination in QDs limiting the efficiency of the above mentioned devices. QDs surface modification during colloidal synthesis or environmental interaction often creates these interfacial trap states and the carriers (electrons or holes) become localized at the lattice defects within the nanocrystal structure. Trap states can also occur due to unsaturated bonds on the nanocrystal surface atoms (surface defect states). Carriers can reside in these trapping sites reducing their mobility in the nanocrystal. Moreover, the radiative recombination efficiency decreases as moving one charge to a trap states reduces the overlap of the electron and hole wave functions in the nanocrystal [2]. Inorganic and organic passivation of unsaturated bonds on the QD surface has been used to enhance fluorescence quantum yields by reducing surface charge trapping

[3]. So far different attempts have been made to study the time scales of carrier trapping and de-trapping on a more fundamental level. Even though both processes are not probed directly, their dynamics have been studied based on the band-edge absorption and fluorescence measurements of ensembles of QDs. The time scale for a carrier to jump from a valence band or conduction band to a trap state is from one to tens of picoseconds. Using transient absorption and fluorescence spectroscopy, the highly non-uniform lifetime of trap states from nanoseconds to microseconds have been inferred from changes in the excited state population of QD ensembles [4,5]. Fluorescence emission at the lower energy side of the band-edge emission attributed to the radiative recombination of trapped carriers have also been measured [6,7].

At the single QD level, carrier trapping causes fluorescence intermittency under continuous excitation. Several experimental [8-22] and theoretical models [23-31] have been proposed to explain this phenomenon. It is accepted in the scientific community that fluorescence blinking is a direct consequence of charge carrier trapping, but the details of the underlying physical mechanism are still under debate. It has been discussed in the literature that two fundamental approaches directly link charge trapping with the non-fluorescence periods of the measured on-off states of the QDs. The first assumes that charge trapping leaves the QD core effectively charged and Auger recombination, which is an efficient non-radiative recombination for charged QDs, determines the low fluorescence quantum yield for a time dictated by the lifetime of the trapped carriers. It is also assumed that the non-radiative recombination of trapped carriers after each excitation can lead to non-fluorescence intervals. In this case, the low fluorescence quantum yield is caused by a fast charge-trapping rate that determines the fluorescence intermittency. The duration of the off-state is then dictated by the time scales of the trapping rate fluctuations. The detail of these explanations and the involved kinetics of the process are still topic of ongoing research [2, 8-31].

To minimize surface trap states, Auger recombination and reduce blinking, QDs are typically coated by a ligand or a wide-bandgap shell. QDs with thicker shells (core/shell QDs) are known to exhibit improved photoluminescence quantum yield of band-edge emission [32-34]. On the other hand, wide-bandgap shells isolate the QDs from the outside environment by confining the wave function of an exciton (electron and hole pair bonded together through electrostatic interaction in a QD nanocrystal), limiting different types of applications [1]. For example, QD based light-emitting diodes would require efficient charge injection into the QDs [35-37]. Hence, an ideal core/shell QD used for optoelectronic applications should avoid intrinsic traps and be sensitive to external carriers with a certain level of drive [3]. Synthesis of such kind of core/shell QDs without trap states for optoelectronic applications is complex. Usually, the shell is epitaxially grown in high quality onto a single crystalline core to remove internal electronic traps and at the core-shell interface. Then, all inorganic-organic interface traps are either excluded by surface treatments or should be isolated by shells with reasonable thickness. The electronic trap at the inorganic-organic interface must be extrinsic to the structural integrity and function of the core/shell QDs. Furthermore, a concrete knowledge on the trapping efficiency as a function of the shell-thickness is required, which so far remains elusive [5, 38-41].

In strongly confined QDs, where the size is smaller than the Bohr excitonic radius, the size-dependent multi-particle Auger non-radiative carrier losses are dominant. When more than one electron-hole pair is excited in a strongly confined QD, Auger decay is extremely efficient due to close proximity between interacting charges and the relaxation of momentum conservation. These lead to extremely fast dynamics on time scales from few to hundreds of picoseconds depending on the QD size [42-44]. In addition to Auger losses and surface traps, the slow spontaneous emission of the band-edge states (few tenth of ns) also hinders their application for high-speed nanoscale optoelectronics.

In this work we report on a complete suppression of trap states emission of a strongly-confined bare-core single QD and enhanced the fluorescence emission from band-edge states by modifying the photonic environment of the QD using plasmonic gold nanocones. Acting as nanoresonators, they provide outstanding possibilities to control the emission dynamics of a single emitter [45,46]. The investigation at a single bare core QD level shows that Auger non-radiative processes are prevented and the radiative decay rate of both exciton and multiexcitonic states (mainly biexcitons) are enhanced by more than two orders of magnitude. The quantum efficiencies of excitonic and biexcitonic emission before and after coupling are experimentally determined by monitoring saturation curves and second-order autocorrelation measurements. The complete suppression of carrier trapping and blinking along with an increase in the quantum efficiency of both excitonic and multiexcitonic states enhance the total emission of the QD. The experimental approaches for coupling, tuning and precise control on the emission dynamics are discussed to obtain more insight on the photophysics of a single QD. In addition, the sensitivity of the bound electron-hole pairs (in a strongly confined bare-core QD, without a shell) to the outside environment enables investigations of unexplored regimes and it is ideal for practical applications such as charge transport and radiative recombination.

### Characterization

We fabricate high-quality plasmonic gold nanocones with dimensions in the 100 nm range using electron beam-induced deposition (EBID) of an organometallic precursor (containing platinum carbide) followed by sputtering deposition of a gold layer [47]. The nanocones exhibit a very sharp tip radius of curvature down to 10 nm. The fabrication technique allows a precise control over size, shape and radius of curvature of the nanocones required for manipulating the photophysics of a single emitter. Figure 1(a) displays a scanning electron-micrograph image of a platinum-carbide based nanocone and a gold nanocone after sputtering deposition. The nanocones are designed to have resonances in the near-infrared region (NIR) to match the emission wavelength of the CdTe QD as shown in Figure 1(b). The NIR region is of special interest as the absorption in gold is smaller. The colloidal QD has a size of  $\sim 5$  nm (smaller than its excitonic Bohr radius  $\sim 7.3$  nm) and it is in the strong-confining regime. This results in well separated electronic states with respect to the available thermal energy leading to stable room-temperature emission properties. The QD emits at a central wavelength of 720 nm and it exhibits slow excitonic and relatively fast biexcitonic lifetime of 22 ns and 6 ns, respectively as shown in Figure 1(c).

To optically access the hybrid quantum system from the top and bottom, gold nanocones are fabricated on a transparent silicon-nitride membrane. A single CdTe QD approaches a nanocone by an atomic force microscope (AFM) probe from the top. QDs are attached to AFM probes by tip functionalization strategies. To prevent quenching of the emitter a silicon nitride tip is preferred to a gold-coated tip. Silanization of the AFM tip offers the advantage that the probe can be functionalized directly without other prior surface preparation. Amine group ( $-\text{NH}_2$ ) is introduced to the tip surface via esterification by reaction of surface silanol group with ethanolamine [ $\text{HO}-(\text{CH}_2)_2-\text{NH}_2$ ]. The CdTe QDs that form colloidal solutions in water are terminated with carboxyl ( $-\text{COOH}$ ) group. This group is activated for direct conjugation to amine through carbodiimide (EDC)-mediated esterification. This enables carboxyl group terminated QDs to be attached to the amine-functionalized tip as shown in Figure 1(d). The dielectric effect of the probe on the emitter is suppressed by using the appropriate ligand length. This offers opportunity to easily image the dipole moment orientation of the single QD at the back focal plane. The determination of the dipole moment orientation of a single QD is an important parameter as it dictates the coupling strength of the core confined electron-hole pairs with the gold nanocone.

The QD attached to the tip of the AFM probe is brought to the near field of a plasmonic nanocone in a controlled way by a closed loop 6-axes piezo stage (Nanowizard<sup>®</sup>4, JPK Instruments AG). The system offers tip positioning and long-time position stability (position noise level < 0.06 nm RMS in the *xy*-plane and < 0.03 nm RMS along the *z*-axis). Analysis of AFM force curves help to precisely determine the QD-nanocone distance with better than 1 nm resolution.

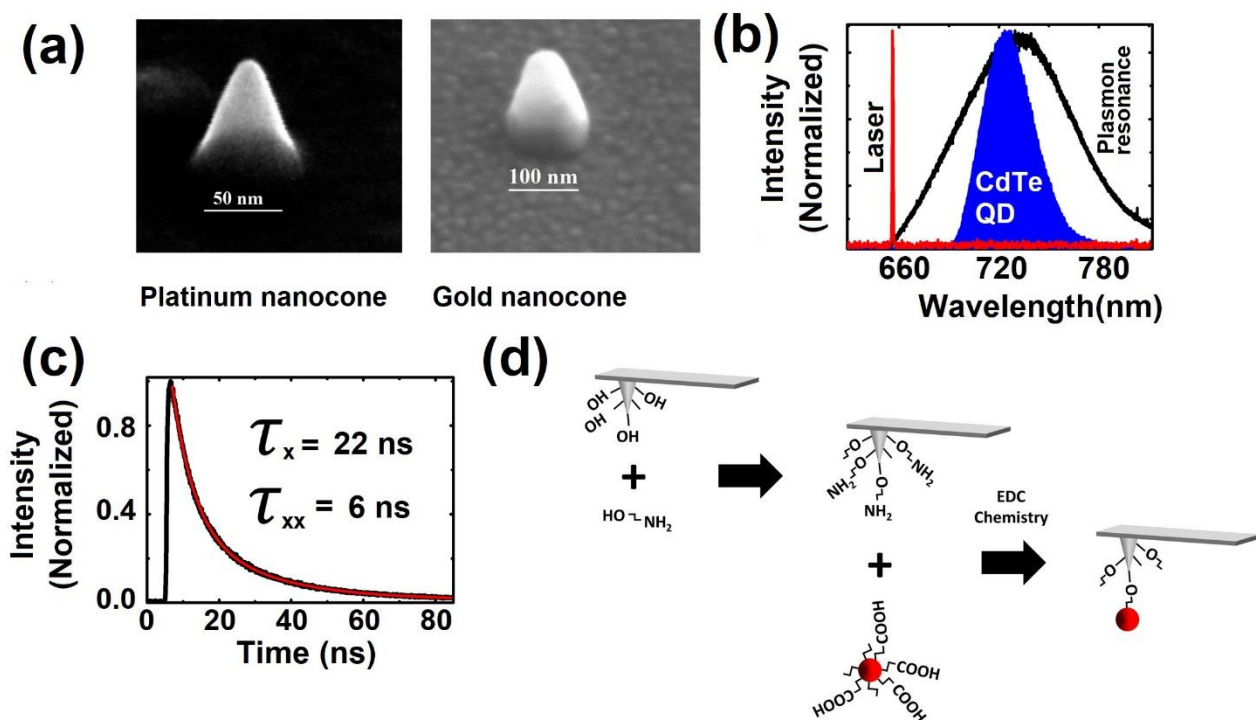


**Figure 1.** (a) Scanning electron micrograph image of platinum based nanocone (left) and gold nanocone (right). (b) Spectral matching of a CdTe QD with a nanocone. The incident laser is detuned from resonance to avoid excitation enhancement. (c) The excited-state lifetime of a CdTe QD placed at the tip of dielectric probe. (d) Functionalization of silicon nitride AFM tips to attach QDs using EDC chemistry.

## Experimental setup

Individual hybrid structures are characterized using a home-built temporal- and spectral resolved confocal-microscopy setup connected to a Hanbury-Brown and Twiss (HBT) interferometer as shown in Figure 2 (a). The sample is excited by a 656 nm cw/pulsed laser at a power < 1mW (PicoQuant, PDL 800-D, LDH-D-C-660) and the emission from the sample is collected via a cover-slip corrected oil-immersion microscope objective (Olympus, 60X, 1.42 NA, 0.15 mm working distance). P-polarized excitation at the location of the hybrid system is implemented to create an electric field component along the cone axis (Figure 2(b)). The spectrometer (Shamrock 500i) is equipped with an electron multiplying CCD (EMCCD) camera (Newton 970, A-DU970P-BVF) that has a quantum efficiency around 90% at the emission wavelength of the QD. Imaging of single CdTe QD is performed using a flippable reflecting mirror that is placed along the optical axis of the setup. After wide-field laser illumination, the collected signal is sent to an EMCCD camera (Princeton Instruments, ProEM-HS: 512 BX3, back-illuminated EMCCD, more than 90% quantum efficiency at the emission wavelength of the QD). The anti-bunching behavior of a single QD is monitored using the second-order intensity autocorrelation. The laser excites the hybrid system and the photoluminescence from the sample is spectrally filtered to suppress the laser. A 50/50 non-polarizing beam splitter sends the

emitted photons to two avalanche photodiodes (APDs) (Micro Photon Devices, 50 cps dark count, < 50p jitter) as shown in Figure 2(c). These detectors are connected to the start-stop time-interval analyzer of a time-correlated single photon counter (TCSPC) (PicoQuant, PicoHarp 300) and the delay between the arrival times of two emitted photons is repeatedly measured and histogrammed with picosecond time resolution. To avoid cross talk between the two APDs, a band pass filter is placed in front of them. The excited-state lifetime is measured using the pulsed mode of the diode laser. The overall instrument response function (IRF) of the setup is less than 70 ps.

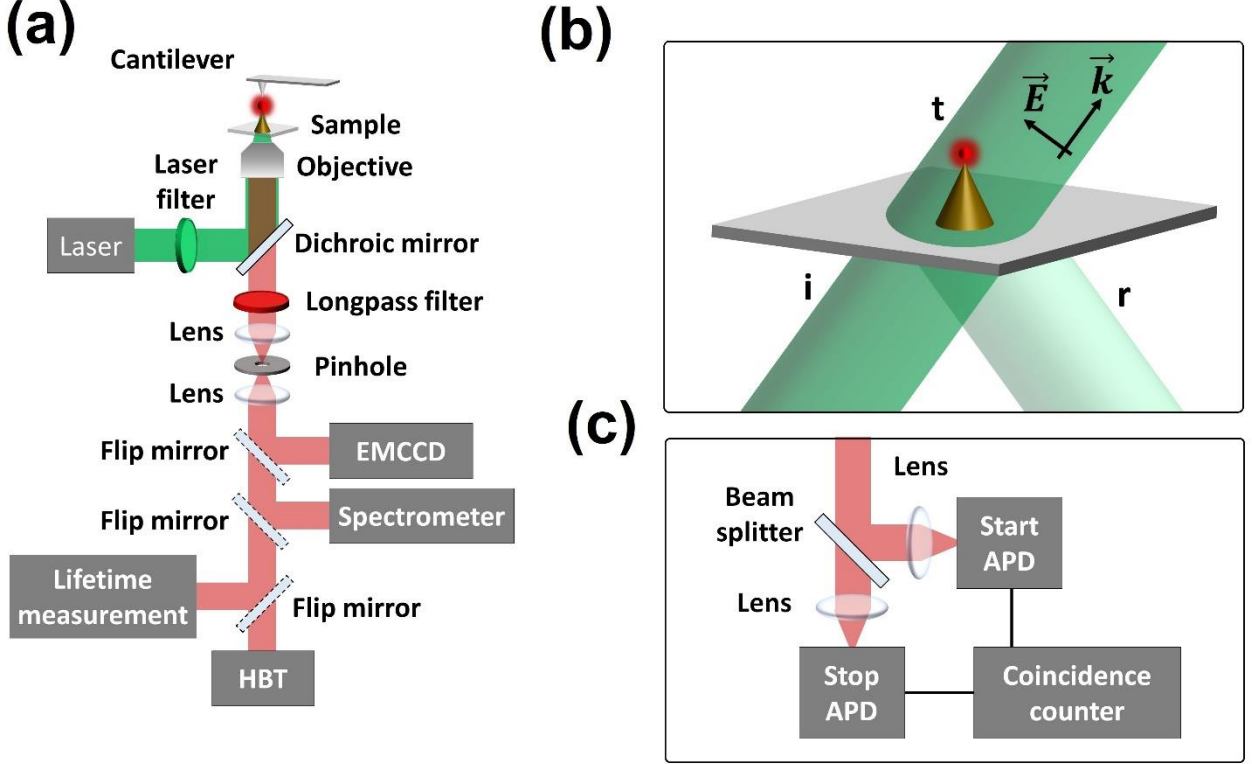


**Figure 2.** (a) Scheme of the experimental setup for imaging, photoluminescence, excited-state lifetime measurements and HBT interferometer. The QD attached to the tip of an AFM probe is brought to the nanocone in nm precision. (b) The incident p-polarized light (i) has a component along the cone axis. Part of light is reflected (r) at the substrate, while the transmitted light (t) effectively excites the vertical dipole moment of the QD. (c) A 50/50 non-polarizing beam splitter sends the emitted photons to two avalanche photodiodes (APDs). The delay between the arrival times of two emitted photons is repeatedly measured and histogrammed with picosecond time resolution.

### QD-nanocone hybrid-quantum system

Figure 3(a) shows the spectrum of a trap-rich single CdTe QD exhibiting both band-edge and trap-state emission. In the measured spectral window more than 74% of the fluorescence signal is obtained from surface-trap emission. The photon statistics is also monitored and it exhibits fluorescence intermittency for continuous excitation as shown in Figure 3(b). This demonstrates the interrogation a single QD (also verified by second-order correlation measurements). A QD with a band-edge state dipole moment orientation along the longitudinal mode of a plasmon nanocone is selected for efficient coupling, as shown in Figure 3(c). The dipole moment of the QD is determined by imaging the back focal plane of the fluorescent light. A doughnut-shape emission pattern is attributed to a dipole moment oriented along the longitudinal axis of the nanocone. The localized surface-plasmon resonance of the nanocone is measured by dark-field spectroscopy with p-polarized white light in a different setup. By defocusing the microscope objective, the doughnut shape of the scattered field corresponds to excitation of the longitudinal plasmon mode (Figure 3(c)). The scattered signal is collected and

normalized for the uneven white light illumination across the broad wavelength range to precisely determine the localized surface-plasmon resonance

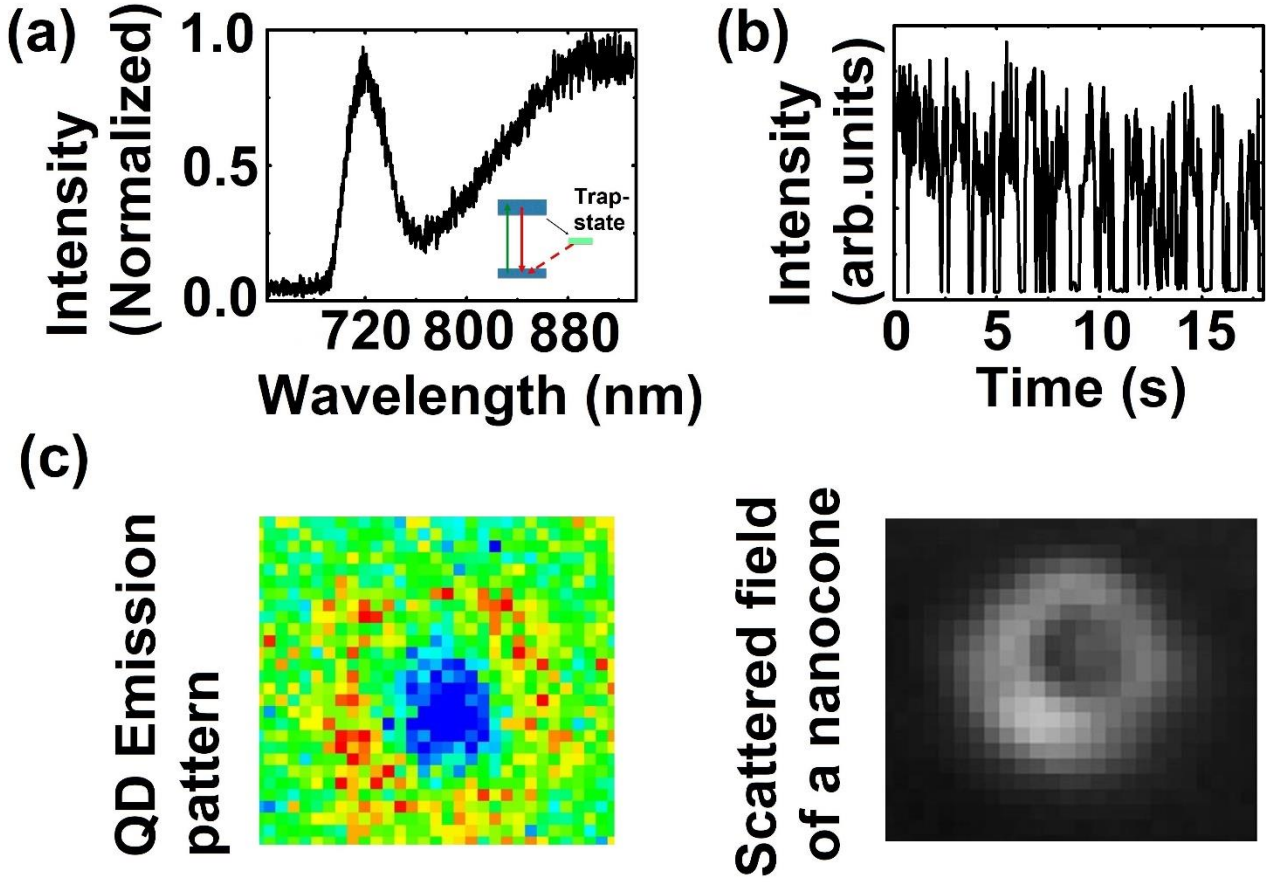


**Figure 3.** (a) Spectrum of a trap-rich single CdTe QD that exhibits both band-edge and surface-state emission. The inset schematically illustrate thee transitions. (b) Fluorescence intermittency of a single CdTe QD under continuous excitation. (c) The doughnut shape of the QD emission pattern is attributed to a dipole moment oriented along the longitudinal axis of the nanocone. The localized plasmon resonance of a nanocone is also precisely determined using dark field spectroscopy and back focal plane imaging.

The excitation laser is detuned from resonance to avoid excitation enhancement (Figure 1(b)). The QD-nanocone distance, polarization of the excitation laser and the dipole orientation of the QD are controlled to modify the coupling strength. Spectrally matching the localized surface-plasmon resonance of a gold nanocone with the band-edge state substantially enhances its emission, while surface-state emission at a wavelength far from the plasmon resonance is significantly suppressed as shown in Figure 4(a) by the red curve. The black curve represents the band-edge and surface-defect state emission of the QD before coupling. When coupling takes place, more than 99% of the emission is associated with the bande-edge transition (red curve). Here, the selective suppression of surface-trap states and the enhancement of the band-edge states is purely a cavity quantum electrodynamics effect.

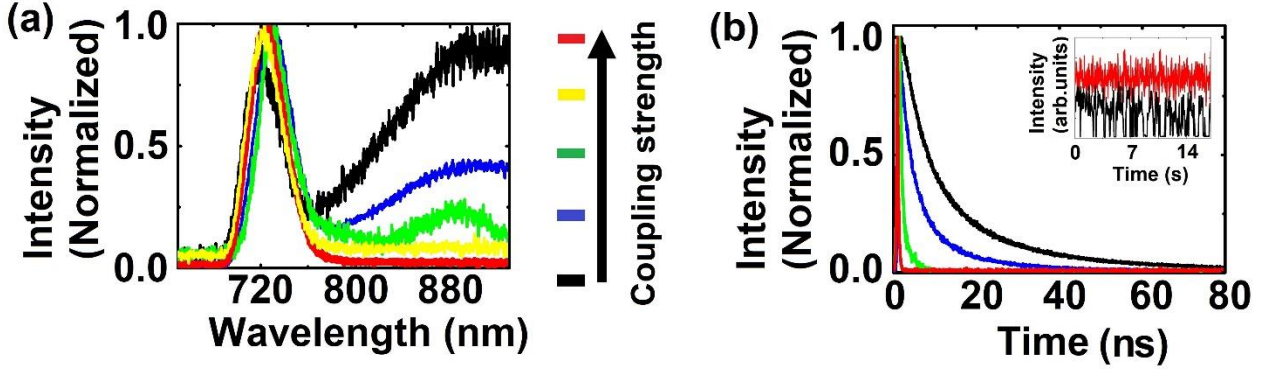


**Figure 4.** (a) The surface defect state of a CdTe QD is modified depending on the coupling strength (QD-nanocone distance and polarization). The QD before coupling (black curve) exhibits defect-state emission. Upon efficient coupling more than 99% of the emission comes from band-edge states (b) Measured excited-state decay curves for different coupling strengths. The extracted lifetime exhibits a shortening of the spontaneous emission rate by two orders of magnitude (red curve). Inset: The fluorescence intermittency of the uncoupled QD (black) is significantly suppressed due to efficient plasmon-coupling (red).

To investigate the modification in the spontaneous emission rate, a 68 ps pulsed laser excites the QD and the emitted photons are detected and histogrammed as a function of delay after the laser pulse. The fluorescence decay curves are fitted by two fluorescence lifetimes. The long lifetime is attributed to excitonic emission channel and the short lifetime to biexcitonic emission pathway. The relative weights of each component are defined by the area under the two exponential curves used to fit the data. By controlled positioning of individual QDs near the gold nanocone, the spontaneous emission rate of excitons and biexcitons are enhanced by more than two orders of magnitude as shown in Figure 4(b). The QD before coupling (black curve) exhibits excitonic and biexcitonic lifetimes of 26.50 ns and 6.88 ns, respectively. By bringing the QD in the near field of a plasmonic nanocone, the excitonic and biexcitonic emission rates are accelerated to 130 ps and 271 ps, respectively (red curve). The IRF (inset) is deconvoluted from the measured lifetime. Further analysis on the emission dynamics (discussed later) shows that these correspond to an enhancement in the radiative decay rate of exciton and biexciton by 676 and 293 folds, respectively.

Recent experiments have also shown very large enhancement factors [48-50], but these are attributed to the overall fluorescence yield obtained, including the effect of excitation enhancement and increase in quantum efficiency. A thousand-fold change in the radiative decay rate was also reported [51,52], based on fluorescence lifetime measurements on ensembles of emitters. So far reports at the single-emitter level are rare [53-55]. In the following a precise experimental determination of the modification in the quantum efficiency, radiative and non-radiative decay rate and the Purcell enhancement of excitonic and biexcitonic emissions of a single QD are determined.

Fluorescence lifetime ( $\tau$ ) measurement provides information about the total decay rate as  $\tau = 1/\gamma_{total}$ . Distinguishing radiative ( $\gamma_r$ ) and nonradiative ( $\gamma_{nr}$ ) decay rates requires information about the quantum efficiency  $\eta = \gamma_r/(\gamma_r + \gamma_{nr})$  both in the absence and presence of the nanostructure. Since  $\eta$  is very sensitive to the environment, each single QD exhibit completely different values. Therefore, the same QD is interrogated during the measurement.

The QD count rate is measured using an APD and the fluorescence signal is imaged using an EMCCD camera. The signal to noise ratio is determined using spatially- and spectrally resolved spectroscopy. The CCD pixel array of the EMCCD attached to the spectrometer (Figure 5(a)) allows to quantify the contribution of scatterers and background signal at the single-photon level. In the weak excitation limit, the QD fluorescence signal  $S_0$  is enhanced due to the presence of the nanocone according to  $S =$

$K_{exc} \cdot K_{\eta} \cdot K_{\delta} \cdot S_0$ , where  $K_{exc}$  is the enhancement of the excitation,  $K_{\eta}$  is the nanocone induced modification of the quantum efficiency and  $K_{\delta}$  refers to the modified collection efficiency of the fluorescence signal in the presence of a nanocone. Note that multiexcitonic emissions has to be considered and the parameters are dependent on the dipole orientation and position of the QD with respect to the nanocone.

As it is shown in Figure 1(b) the excitation laser is blue-detuned from the matched spectral region of the QD and plasmon resonance. Therefore, there is no substantial excitation enhancement and  $K_{exc}$  to be in the order of unity. A high collection efficiency cover-slip corrected oil-immersion microscope objective (Olympus, 60X, 1.42 NA) also leads to near unity modified collection efficiency  $K_{\delta}$ . But the determination of  $K_{\eta}$  and separating  $\gamma_r$  and  $\gamma_{nr}$  of excitonic and biexcitonic emission pathways will require further measurement as discussed below.

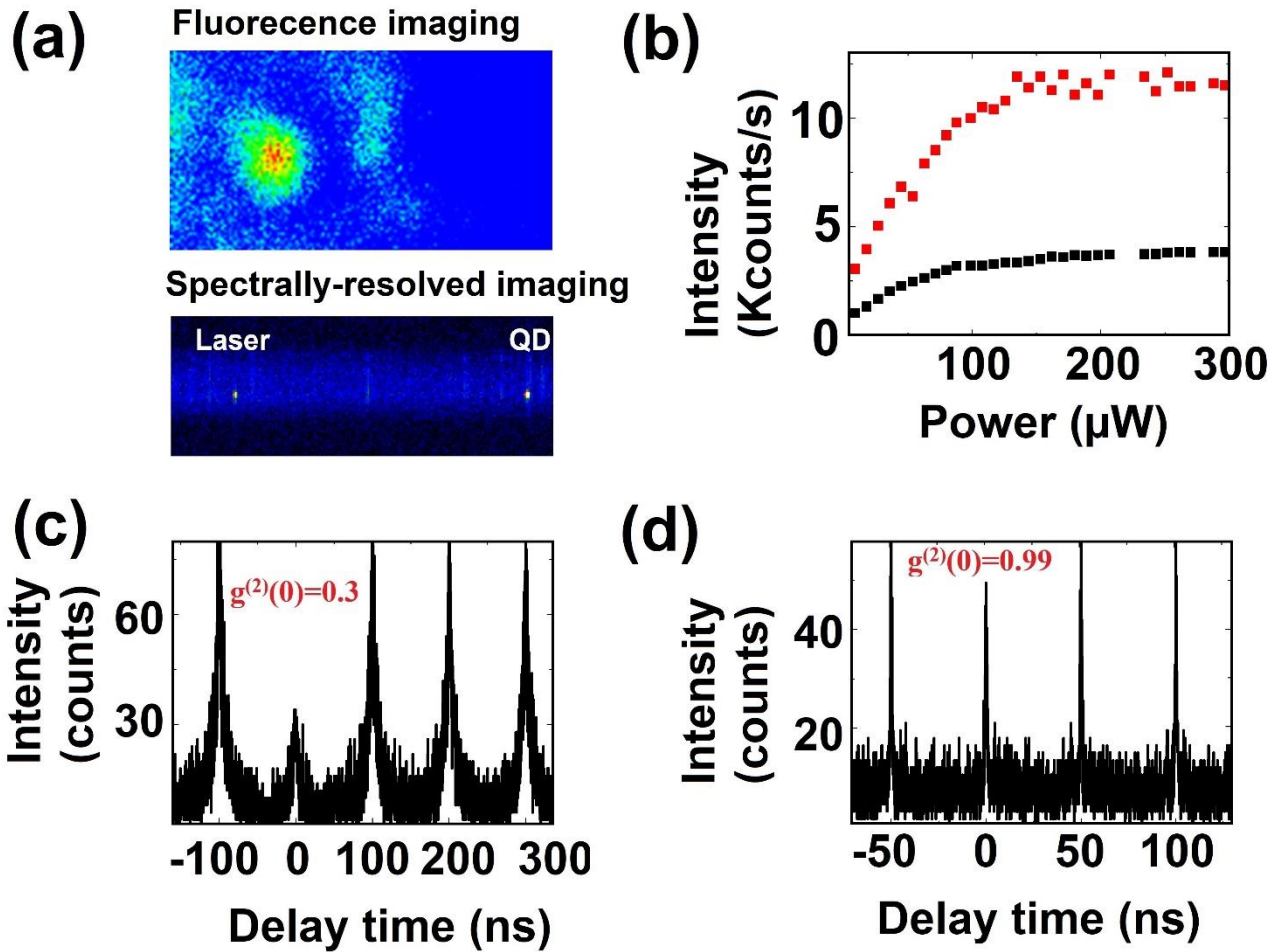


**Figure 5.** (a) The fluorescence signal is imaged using an EMCCD and the signal to noise is determined using the CCD pixel array of the EMCCD attached to the spectrometer. One of the laser filter is removed for imaging the laser line. (b) Total fluorescence signal from a OD as a function of the excitation power before coupling (black curve) and after coupling (red curve). (c) Second-order autocorrelation function of the QD before coupling. (d) Second-order autocorrelation function of the QD after coupling.

The quantum efficiency  $\eta$  is the ratio of the number of emitted photons to the number of excitations. Unlike the determination of  $\eta$  for an ensemble of QDs (e.g., using an integrating sphere), precise determination of the number of absorbed and emitted photons of a single QD is not trivial. In this work

we saturate the single QD using a low repetition-rate (1 MHz) laser, so that each incident laser pulse leads to an excitation (each pulse finds the QD in the ground state after the previous excitation). Moreover, this avoids complexity caused by the unavoidable QD dark states. The black curve on Figure 5(b) shows the saturation curve of the emitter to quantify the total emission rate of the QD at the tip of the probe (before coupling) as a function of the excitation power. Since the recorded signal has both excitons and biexcitons contribution, the fluorescence decay curve is also recorded at different powers until the contribution from the exciton channel is constant. It is found that beyond 100  $\mu\text{W}$  the excitonic emission is saturated and the fluorescence signal becomes  $S_0 = 2.8$  kcps. Taking into consideration the overall detection efficiency  $\beta = 2\%$  of our setup, the number of emitted photons can be deduced from  $S_0/\beta$ . Hence, the excitonic quantum efficiency in the absence of nanocone turns out to be  $\eta_0^x \approx 14\%$ . This information directly tells that the radiative and non-radiative lifetime of the exciton before coupling are  $\tau_{0,r}^x = 189.3$  ns and  $\tau_{0,nr}^x = 30.8$  ns, respectively. The biexcitonic quantum efficiency  $\eta_0^{xx}$  is determined using the second-order autocorrelation measurement at zero delay time. Using the Hanbury-Brown and Twiss photo autocorrelation measurement, one can use of the relation  $g_0^{(2)}(0) = \eta_0^{xx}/\eta_0^x$  to determine the biexcitonic quantum efficiency [56,57]. The autocorrelation is measured at 10 MHz repetition-rate to decrease the acquisition time required to develop enough representative histogram. As shown in Figure 5(c) we find  $g_0^{(2)}(0) = 0.3$ , corresponding to a biexcitonic quantum efficiency of  $\eta_0^{xx} = 4.2\%$ . Hence, the radiative and non-radiative lifetime of the biexciton are  $\tau_{0,r}^{xx} = 163.8$  ns and  $\tau_{0,nr}^{xx} = 7.18$  ns, respectively.

For the QD positioned at the tip of the nanocone, the total signal is affected by enhanced radiative contribution from excitons and biexcitons. We find that excitonic saturation occurs at a power of 116  $\mu\text{W}$  as shown in Figure 5(b) (red curve) and the exciton fluorescence signal becomes  $S = 9.2$  kcps. Taking into consideration the same collection efficiency, the excitonic quantum efficiency turns out to be  $\eta_c^x = 46\%$ , which is more than 3 time higher than the uncoupled QD. This corresponds to an excitonic radiative and non-radiative lifetimes of  $\tau_{c,r}^x = 0.28$  ns and  $\tau_{c,nr}^x = 0.24$  ns, respectively. Therefore, the excitonic radiative decay enhancement factor becomes  $F_r^x = \gamma_{c,r}^x/\gamma_{0,r}^x = 676$ . The biexcitonic quantum efficiency is similarly inferred from the second-order correlation measurement (see Figure 5(d)) and it turns out to be  $\eta_c^{xx} = 45.54\%$ . Thus, the biexcitonic radiative and non-radiative lifetimes become  $\tau_{c,r}^{xx} = 0.56$  ns and  $\tau_{c,nr}^{xx} = 0.5$  ns, respectively, during coupling, and the biexcitonic radiative decay enhancement factor is  $F_r^{xx} = \gamma_{c,r}^{xx}/\gamma_{0,r}^{xx} = 293$ . These results show that efficient coupling completely changes the QD photophysics and turn it into a bright emitter.

In conclusion, we have reported complete suppression of surface-trap emission of a bare QD solely based on plasmonic coupling. Moreover, we have shown that a strong increase of the radiative excitonic and multiexcitonic transitions (mainly biexciton) suppresses fluorescence intermittency and boost the QD brightness. The biexcitonic enhancement can be mainly attributed to a faster photon emission rate as compared to competitive Auger and other non-radiative rates. The nanoscale size of the hybrid system allows integration into micro- and nano structures (e.g., microresonators and planar antennas) for achieving large collection efficiency and directionality [58-60]. This alternative approach can also be used to shape the emission spectra of a fluorescence molecule by selectively favouring transitions to a specific vibrational ground state [61]. In addition to fluorescence enhancement, huge radiative decay rates are interesting in solid-state spectroscopy as the enhancement of  $\gamma_r$  is directly related to a larger extinction cross section, with an impact on the field of coherent plasmonics [62,63].

## Acknowledgements

The authors gratefully acknowledge financial support from the University of Siegen, Germany, and the Italian Institute of Technology (IIT), Italy. This article is based upon work from COST Action MP1403 “Nanoscale Quantum Optics,” supported by COST (European Cooperation in Science and Technology). A. Flatae would like to thank F. Dinelli for advice on the AFM techniques, M. Ardini and M. Mousavi for advice on functionalization protocols and P. Reuschel for technical assistance.

**Keywords:** colloidal quantum dots • radiative decay rate • surface defect state • plasmonic nanostructures • hybrid quantum system

## References

- [1] D.V. Talapin, J.S. Lee, M.V. Kovalenko, E.V. Shevchenko, *Chem. Rev.* **2010**, *110*, 389-458.
- [2] A.A. Cordones, S.R. Leone, *Chem. Soc. Rev.* **2013**, *42*, 3209-3221.
- [3] X. Peng, M.C. Schlamp, A.V. Kadavanich, A.P. Alivisatos, *J. Am. Chem. Soc.* **1997**, *119*, 7019-7029.
- [4] K.E. Knowles, E.A. McArthur, E. A. Weiss, *ACS Nano*, **2011**, *5*, 2026-2035.
- [5] M. Jones, S. S. Lo, G. D. Scholes, *PNAS*, **2009**, *106*, 3011-3016.
- [6] C. Burda, S. Link, M. Mohamed, M. El-sayed, *J. Phys. Chem. B* **2001**, *105*, 12286-12292.
- [7] D.F. Underwood, T. Kippeny, S.J. Rosenthal, *J. Phys. Chem. B* **2001**, *105*, 436-443.
- [8] K.T. Shimizu, R.G. Neuhauser, C.A. Leatherdale, S.A. Empedocles, W.K. Woo, M.G. Bawendi, *Phys. Rev. B* **2001**, *63*, 205316.
- [9] B.R. Fisher, H.J. Eisler, N.E. Stott, M.G. Bawendi, *J. Phys. Chem. B* **2004**, *108*, 143-148.
- [10] X. Brokmann, J.P. Hermier, G. Messin, P. Desbiolles, J.P. Bouchaud, M. Dahan, *Phys. Rev. Lett.* **2003**, *90*, 120601.
- [11] M. Pelton, D.G. Grier, P. Guyot-Sionnest, *Appl. Phys. Lett.* **2004**, *85*, 819-821.
- [12] R. Verberk, A.M. van Oijen, M. Orrit, *Phys. Rev. B* **2002**, *66*, 233202.
- [13] G. Schlegel, J. Bohnenberger, I. Potapova, A. Mews, *Phys. Rev. Lett.* **2003**, *88*, 137401.
- [14] R. Verberk, M. Orrit, *J. Chem. Phys.* **2003**, *119*, 2214-2222.
- [15] M. Kuno, D.P. Fromm, H.F. Hamann, A. Gallagher, D.J. Nesbitt, *J. Chem. Phys.* **2001**, *115*, 1028-1040.
- [16] K.T. Shimizu, W.K. Woo, B.R. Fisher, H.J. Eisler, M.G. Bawendi, *Phys. Rev. Lett.* **2002**, *89*, 117401.
- [17] I.H. Chung, M.G. Bawendi, *Phys. Rev. B* **2004**, *70*, 165304.
- [18] I. Chung, J.B. Witkoskie, J. Cao, M.G. Bawendi, *Phys. Rev. E* **2006**, *73*, 011106.
- [19] M. Kuno, D.P. Fromm, S.T. Johnson, A. Gallagher, D.J. Nesbitt, *Phys. Rev. B* **2003**, *67*, 125304.
- [20] G. Messin, J.P. Hermier, E. Giacobino, P. Desbiolles, M. Dahan, *Opt. Lett.* **2001**, *26*, 1891-1893.
- [21] A. Issac, C. von Borczyskowski, F. Cichos, *Phys. Rev. B* **2005**, *71*, 161302.
- [22] V. Biju, Y. Makita, T. Nagase, Y. Yamaoka, H. Yokoyama, Y. Baba, H. Ishikawa, *J. Phys. Chem. B* **2005**, *109*, 14350-14355.
- [23] J. Tang, R.A. Marcus, *Phys. Rev. Lett.* **2005**, *95*, 107401-107404.
- [24] A.L. Efros, M. Rosen, *Phys. Rev. Lett.* **1997**, *78*, 1110-1113.
- [25] J. Tang, R.A. Marcus, *J. Chem. Phys.* **2005**, *123*, 054704.
- [26] G. Margolin, E. Barkai, *J. Chem. Phys.* **2004**, *121*, 1566-1577.
- [27] G. Margolin, G.V. Protasenko, M. Kuno, E. Barkai, *Adv. Chem. Phys.* **2006**, *133*, 327-356.
- [28] J. Tang, R.A. Marcus, *Phys. Rev. Lett.* **2005**, *95*, 107401.
- [29] P.A. Frantsuzov, R.A. Marcus, *Phys. Rev. B* **2005**, *72*, 155321.
- [30] G. Margolin, E. Barkai, *Phys. Rev. Lett.* **2005**, *94*, 080601.
- [31] S. Bianco, P. Grigolini, P. Paradisi, *J. Chem. Phys.* **2005**, *123*, 174704.
- [32] L. Spanhel, M. Haase, H. Weller, A. Henglein, *J. Am. Chem. Soc.* **1987**, *109*, 5649-5655.
- [33] A.R. Kortan, R. Hull, R.L. Opila, M.L. Steigerwald, P. J. Carroll, L.E. Brus, *J. Am. Chem. Soc.* **1990**, *112*, 1327-1332.
- [34] M.A. Hines, P. Guyot-Sionnest, *J. Phys. Chem.* **1996**, *100*, 468-471.

- [35] V.L. Colvin, M. C. Schlamp, A.P. Alivisatos, *Nature* **1994**, 370, 354-357.
- [36] S. Coe, W.K. Woo, M. Bawendi, V. Bulovic, *Nature* **2002**, 420, 800-803.
- [37] X. Dai, Z. Zhang, Y. Jin, Y. Niu, H. Cao, X. Liang, L. Chen, J. Wang, X. Peng, *Nature* **2014**, 515, 96-99.
- [38] J. McBride, J. Treadway, L. C. Feldman, S.J. Pennycook, S.J. Rosenthal, *Nano Lett.* **2006**, 6, 1496-1501.
- [39] P. Maity, T. Debnath, H.N. Ghosh, *J. Phys. Chem. C* **2015**, 119, 10785-10792.
- [40] J.J. Li, Y. A. Wang, W. Guo, J. C. Keay, T. D. Mishima, M. B. Johnson, X. Peng, *J. Am. Chem. Soc.* **2003**, 125, 12567-12575.
- [41] C. Pu, X. Peng, *J. Am. Chem. Soc.* **2016**, 138, 8134-8142.
- [42] V.I. Klimov, A.A. Mikhailovsky, D.W. McBranch, C.A. Leatherdale, M.G. Bawendi, *Science*, **2000**, 287, 1011-1013.
- [43] V.I. Klimov, *Annu. Rev. Condens. Matter Phys.* **2014**, 5, 285-316.
- [44] A. Pandey, P. Guyot-Sionnest, *J. Chem. Phys.* **2007**, 127, 111104.
- [45] M. Agio, *Nanoscale* **2012**, 4, 692-706.
- [46] A. Mohammadi, F. Kaminski, V. Sandoghdar, M. Agio, *J. Phys. Chem. C* **2010**, 114, 7372-7377.
- [47] A.M. Flatae, F. Tantussi, G.C. Messina, A. Mohammadi, F. De Angelis, M. Agio, *Adv. Optical Mater.* **2017**, 5, 1700586.
- [48] A. Kinkhabwala, Z. Yu, S. Fan, Y. Avlasevich, K. Muellen, W. E. Moerner, *Nat. Photonics* **2009**, 3, 654-657.
- [49] S. Khatua, P. M. R. Paulo, H. Yuan, A. Gupta, P. Zijlstra, M. Orrit, *ACS Nano* **2014**, 8, 4440-4449.
- [50] T. B. Hoang, G. M. Akselrod, C. Argyropoulos, J. Huang, D. R. Smith, M. H. Mikkelsen, *Nat. Commun.* **2015**, 6, 7788.
- [51] K.J. Russell, T.L. Liu, S. Cui, E. Yu, *Nat. Photonics* **2012**, 6, 459-462.
- [52] G. M. Akselrod, C. Argyropoulos, T. B. Hoang, C. Ciraci, C. Fang, J. Huang, D. R. Smith, M. H. Mikkelsen, *Nat. Photonics* **2014**, 8, 835-840.
- [53] T. B. Hoang, G. M. Akselrod, M. H. Mikkelsen, *Nano Lett.* **2016**, 16, 270-275.
- [54] K-G. Lee, H. Eghlidi, X-W. Chen, A. Renn, S. Goetzinger, V. Sandoghdar, *Opt. Exp.* **2012**, 20, 23331-23338.
- [55] K. Matsuzaki, S. Vassant, H.-W. Liu, A. Dutschke, B. Hoffmann, X. Chen, S. Christiansen, M.R. Buck, J.A. Hollingsworth, S. Goetzinger, V. Sandoghdar, *Sci. Rep.* **2017**, 7, 42307.
- [56] G. Nair, J. Zhao, M.G. Bawendi, *Nano Lett.* **2011**, 11, 1136-1140.
- [57] Y.S. Park, A.V. Malko, J. Vela, Y. Chen, Y. Ghosh, F. Garcia-Santamaria, J.A. Hollingsworth, V.I. Klimov, H. Htoon, *Phys. Rev. Lett.* **2011**, 106, 187401.
- [58] K.G. Lee, X.W. Chen, H. Eghlidi, P. Kukura, R. Lettow, A. Renn, V. Sandoghdar, S. Götzinger, *Nat. Photonics* **2011**, 5, 166-169.
- [59] X.L. Chu, T.J.K. Brenner, X.W. Chen, Y. Ghosh, J.A. Hollingsworth, V. Sandoghdar, S. Götzinger, *Optica* **2014**, 1, 203-208.
- [60] H. Galal, M. Agio, *Opt. Mater. Express*, **2017**, 7, 1634-1646.
- [61] M. Ringler, A. Schwemer, M. Wunderlich, A. Nichtl, T.A. Klar, J. Feldmann, *Phys. Rev. Lett.* **2008**, 100, 203002.
- [62] X.W. Chen, V. Sandoghdar, M. Agio, *Phys. Rev. Lett.* **2013**, 110, 153605.
- [63] R. Chikkaraddy, B. de Nijs, F. Benz, S.J. Barrow, O. A. Scherman, E. Rosta, A. Demetriadou, P. Fox, O. Hess, J.J. Baumberg, *Nature* **2016**, 535, 127-130.